J|A|C|S
ARTICLES
Published on Web 05/13/2006

Determination of the Oligomeric Number and Intermolecular Distances of Membrane Protein Assemblies by Anisotropic ^{1}H-Driven Spin Diffusion NMR Spectroscopy

Wenbin Luo and Mei Hong*

Contribution from the Department of Chemistry, Iowa State University, Gilman 0108, Ames, Iowa 50011

Received January 17, 2006; E-mail: mhong@iastate.edu

Abstract: Determination of the high-resolution quaternary structure of oligomeric membrane proteins requires knowledge of both the oligomeric number and intermolecular distances. The centerband-only detection of exchange (CODEX) technique has been shown to enable the extraction of the oligomeric number through the equilibrium exchange intensity at long mixing times. To obtain quantitative distances, we now provide an analysis of the mixing-time-dependent CODEX intensities using the ^{1}H-driven spin diffusion theory. The exchange curve is fit to a rate equation, where the rate constants are proportional to the square of the dipolar coupling and the spectral overlap integral between the exchanging spins. Using a number of ^{13}C- and ^{19}F-labeled crystalline model compounds with known intermolecular distances, we empirically determined the overlap integrals of ^{13}C and ^{19}F CODEX for specific spinning speeds and chemical shift anisotropies. These consensus overlap integral values can be applied to structurally unknown systems to determine distances. Applying the ^{19}F CODEX experiment and analysis, we studied the transmembrane peptide of the M2 protein (M2TMP) of influenza A virus bound to 1,2-dimyristoyl-*sn*-glycero-3-phosphatidylcholine bilayers. The experiment proved for the first time that M2TMP associates as tetramers in lipid bilayers, similar to its oligomeric state in detergent micelles. Moreover, the nearest-neighbor interhelical F−F distance between (4-^{19}F)Phe30 is 7.9−9.5 Å. This distance constrains the orientation and the packing of the helices in the tetrameric bundle and supports the structural model derived from previous solid-state NMR ^{15}N orientational data. Thus, the CODEX technique presents a general method for determining the oligomeric number and intermolecular distances in the ∼10 Å range in membrane proteins and other complex biological assemblies.

1. Introduction

One of the remaining challenges in structural biology today is the determination of the quaternary structure of membrane proteins. Many membrane proteins such as ion channels oligomerize with well-defined stoichiometry and structure to carry out their function. Elucidating the intermolecular packing of these proteins is essential not only for deciphering the structure−function relations of specific proteins but also for understanding the general principles of membrane protein folding.[1,2] To determine the oligomeric structures, intermolecular distance constraints are essential. Many solid-state NMR techniques utilizing dipolar recoupling under magic-angle spinning (MAS)[3−6] have been developed to measure distances. However, most of these techniques yield only relatively short internuclear distances of ∼5 Å. The determination of long-range distances still remains a challenge.

Dipolar-driven spin diffusion NMR is a robust approach for obtaining semi-quantitative homonuclear distances. Both direct ^{1}H−^{1}H spin diffusion and ^{1}H-driven X-nucleus (X = ^{13}C, ^{19}F, etc.) spin diffusion have been analyzed and employed for distance determination in small molecules[7,8] and in isotopically labeled proteins.[9−12] Because of the lack of ^{1}H decoupling during the mixing time and the long T_1 relaxation time of many X nuclei, measuring long-range distances with spin diffusion is straightforward, simply involving lengthening the mixing time. As a new member of this family, the centerband-only detection of exchange (CODEX) technique, which is based on ^{1}H-driven anisotropic spin diffusion, has been shown to enable spin counting, i.e., the determination of the oligomeric number of proteins.[13] We now show that it can also be used to extract intermolecular distances and is thus a particularly effective tool for elucidating the oligomeric structure of membrane proteins.

(1) Popot, J. L.; Engelman, D. M. *Biochemistry* **1990**, *29*, 4031−4037.
(2) DeGrado, W. F.; Gratkowski, H.; Lear, J. D. *Protein Sci.* **2003**, *12*, 647−665.
(3) Dusold, S.; Sebald, A. *Annu. Rep. NMR Spectrosc.* **2000**, *41*, 185−264.
(4) Antzutkin, O. N. In *Solid-state NMR spectroscopy principles and applications*; Duer, M. J., Ed.; Blackwell Sciences, Inc.: Oxford, 2002; pp 280−390.
(5) Gullion, T.; Schaefer, J. *J. Magn. Reson.* **1989**, *81*, 196−200.
(6) Raleigh, D. P.; Creuzet, F.; Gupta, S. K. D.; Levitt, M. H.; Griffin, R. G. *J. Am. Chem. Soc.* **1989**, *111*, 4502−4503.
(7) Bronniman, C. E.; Szeverenyi, N. M.; Maciel, G. E. *J. Chem. Phys.* **1983**, *79*, 3694−3700.
(8) Tekely, P.; Potrzebowski, M. J.; Dusausoy, Y.; Luz, Z. *Chem. Phys. Lett.* **1998**, *291*, 471−479.
(9) Castellani, F.; vanRossum, B.; Diehl, A.; Schubert, M.; Rehbein, K.; Oschkinat, H. *Nature* **2002**, *420*, 98−102.
(10) Luo, W.; Yao, X. L.; Hong, M. *J. Am. Chem. Soc.* **2005**, *127*, 6402−6408.
(11) Lange, A.; Seidel, K.; Verdier, L.; Luca, S.; Baldus, M. *J. Am. Chem. Soc.* **2003**, *125*, 12640−12648.
(12) Huster, D.; Yao, X. L.; Hong, M. *J. Am. Chem. Soc.* **2002**, *124*, 874−883.

10.1021/ja0603406 CCC: $33.50

The principle of the CODEX technique[14,15] for spin counting is magnetization exchange between orientationally different and singly labeled molecules. Two rotor-synchronized π-pulse trains recouple the orientation-dependent chemical shift anisotropy (CSA) of X spins under MAS. Between the two π-pulse trains, ^{1}H-driven X spin diffusion occurs between chemically equivalent but orientationally inequivalent spins, causing a change of the CSA frequency, which prevents the complete refocusing of a stimulated echo at the end of the second π-pulse train. At long exchange mixing times, the initial magnetization is equally distributed among n orientations in the cluster, reducing the CODEX echo intensity to $1/n$. Thus, the equilibrium value of the exchange intensity gives the oligomeric number of aggregating proteins or the number of magnetically inequivalent molecules in a crystal unit cell.[13] Using ^{19}F CODEX, we showed that protegrin-1, a β-sheet antimicrobial peptide, forms dimers in POPC bilayers.[13]

While the CODEX equilibrium intensity permits spin counting, the time-dependent CODEX intensity decay contains distance information, since the homonuclear X−X dipolar coupling that drives magnetization exchange scales with distance (r) as $1/r^3$. Thus, it is desirable to extend the capability of the CODEX technique beyond spin counting to include distance determination. According to the ^{1}H-driven spin diffusion theory, the rate of magnetization exchange depends on the dipolar coupling and the spectral overlap integral, the precise value of which is difficult to predict from first principles. Thus, here we adopt an empirical approach of calibrating the overlap integral using model compounds with known internuclear distances, and we show that consensus overlap integral values can be obtained for specific chemical functional groups and experimental conditions. These consensus overlap integral values can then be used for distance determination of structurally unknown molecular assemblies.

As a first application of the ^{19}F CODEX experiment and analysis, we investigate the transmembrane peptide of the M2 protein (M2TMP) of influenza A virus. The 97-residue M2 protein forms proton-conducting channels that initiate the dissociation of the viral RNA/protein complex and the fusion of the viral membrane with the endosomal wall.[16,17] Various studies showed that the active M2 ion channel is a tetramer in vivo[18] and the transmembrane domain also forms a tetramer in detergent micelles.[19,20] However, the oligomeric state of the peptide in the lipid bilayer has not been directly determined. The structure of the M2TMP helical bundle has been investigated by Cys scanning and conductivity measurements,[21] and the orientation of the peptide has been accurately measured by ^{15}N NMR.[22] Beside these, only a single short distance has been reported on this peptide.[23] Thus, currently the highest-resolution structural information about the M2 helical bundle concerns the monomer and the backbone. Few constraints about the helix−helix packing and the side-chain conformation are available.

In this study, we first use carbonyl (^{13}C′)-labeled and ^{19}F-labeled model compounds with known intermolecular distances to extract consensus overlap integral values for the ^{13}C and ^{19}F CODEX experiments. We then apply the ^{19}F CODEX experiment to determine the oligomeric number of M2TMP directly in lipid bilayers for the first time. Moreover, we extract the interhelical distance between Phe30 residues from the ^{19}F CODEX curves and show that this distance provides a sensitive restraint to the orientation of the peptide and the interhelical separation of the bundle. This is the first time that the oligomeric number and a long intermolecular distance are determined for this homo-oligomeric helical bundle in lipid bilayers.

2. Materials and Methods

Sample Preparation. Isotopically labeled model compounds, including ^{13}C′-Gly, ^{13}C′-Leu, ^{13}C′-Phe, 5-^{19}F-Trp, and 4-^{19}F-2′-nitroacetanilide, were purchased from Cambridge Isotope Laboratories (Andover, MA) and Sigma (St. Louis, MO). 1,2-Dimyristoyl-*sn*-glycero-3-phosphatidylcholine (DMPC) was obtained from Avanti Polar Lipids (Alabaster, AL). The fluorinated M2 peptide, A30F-M2TMP, where Ala30 was replaced by (4-^{19}F)Phe, was custom synthesized by SynPep Corp. (Dublin, CA) using standard Fmoc chemistry. The amino acid sequence is NH_2-Ser22-Ser23-Asp24-Pro25-Leu26-Val27-Val28-Ala29-(4-^{19}F)Phe30-Ser31-Ile32-Ile33-Gly34-Ile35-Leu36-His37-Leu38-Ile39-Leu40-Trp41-Ile42-Leu43-Asp44-Arg45-Leu46-COOH. The A30F mutation was shown by analytical ultracentrifugation experiments to stabilize the tetramer in DPC micelles.[20] The purified A30F-M2TMP was repeatedly washed in dilute HCl solution to remove residual trifluoroacetate (TFA) salt, until no TFA signal (−75 ppm) was observed in the ^{19}F solution NMR spectrum.

Membrane-bound A30F-M2TMP was prepared using a procedure similar to that reported by Cross and co-workers.[23] Large unilamellar DMPC vesicles were prepared by dissolving DMPC lipids in 5 mM Na_2HPO_4/NaH_2PO_4 buffer at 30 °C (pH 7), vortexing, freeze−thawing, and extruding the solution through polycarbonate filter membranes with 1 μm pores at 27 °C. Purified A30F-M2TMP was dissolved in the DMPC vesicle solution at a P:L molar ratio of 1:15. The membrane mixture was vortexed, sonicated, and incubated at 30 °C for 2 days to facilitate peptide reconstitution. The mixture was then centrifuged at 150000*g* for 2 h at 28 °C, and the pellet was collected. Photometric assay of the supernatant[24] showed that 90% of the peptide was reconstituted into the membrane. The pellet was transferred to a 4 mm rotor and incubated at 30 °C for 2 days before the NMR experiments.

Solid-State NMR Experiments. CODEX experiments were carried out on a Bruker DSX-400 spectrometer (Karlsruhe, Germany) operating at a resonance frequency of 400.49 MHz for ^{1}H, 376.8 MHz for ^{19}F, and 100.71 MHz for ^{13}C, using MAS probes equipped with 4 mm spinner modules. The spinning speed was 8 kHz for the ^{19}F experiments and 2.5−10 kHz for the ^{13}C experiments. The ^{19}F CODEX experiments used a H/F/X probe that allows simultaneous tuning of the ^{1}H and ^{19}F frequencies on a single channel through a combiner/splitter assembly. Experiments on M2TMP were conducted at 240 K using air cooled through a Kinetics Thermal Systems XR Air-Jet Cooler (Stone Ridge,

(13) Buffy, J. J.; Waring, A. J.; Hong, M. *J. Am. Chem. Soc.* **2005**, *127*, 4477−4483.
(14) deAzevedo, E. R.; Bonagamba, T. J.; Hu, W.; Schmidt-Rohr, K. *J. Am. Chem. Soc.* **1999**, *121*, 8411−8412.
(15) Schmidt-Rohr, K.; deAzevedo, E. R.; Bonagamba, T. J. In *Encyclopedia of NMR*; Grant, D. M., Harris, R. K., Eds.; John Wiley & Sons: Chichester, 2002.
(16) Lamb, R. A.; Holsinger, K. J.; Pinto, L. H. In *Cellular Receptors of Animal Viruses*; Wemmer, E., Ed.; Cold Spring Harbor Laboratory Press: Plainview, NY, 1994; pp 303−321.
(17) Duff, K. C.; Ashley, R. H. *Virology* **1992**, *190*, 485−489.
(18) Sakaguchi, T.; Tu, Q.; Pinto, L. H.; Lamb, R. A. *Proc. Natl. Acad. Sci. U.S.A.* **1997**, *94*, 5000−5005.
(19) Salom, D.; Hill, B. R.; Lear, J. D.; DeGrado, W. F. *Biochemistry* **2000**, *39*, 14160−14170.
(20) Howard, K. P.; Lear, J. D.; DeGrado, W. F. *Proc. Natl. Acad. Sci. U.S.A.* **2002**, *99*, 8568−8572.
(21) Pinto, L. H.; Dieckmann, G. R.; Gandhi, C. S.; Papworth, C. G.; Braman, J.; Shaughnessy, M. A.; Lear, J. D.; Lamb, R. A.; DeGrado, W. F. *Proc. Natl. Acad. Sci. U.S.A.* **1997**, *94*, 11301−11306.
(22) Wang, J.; Kim, S.; Kovacs, F.; Cross, T. A. *Protein Sci.* **2001**, *10*, 2241−2250.
(23) Nishimura, K.; Kim, S.; Zhang, L.; Cross, T. A. *Biochemistry* **2002**, *41*, 13170−13177.
(24) Pace, C. N.; Vajdos, F.; Fee, L.; Grimsley, G.; Gray, T. *Protein Sci.* **1995**, *4*, 2411−2423.

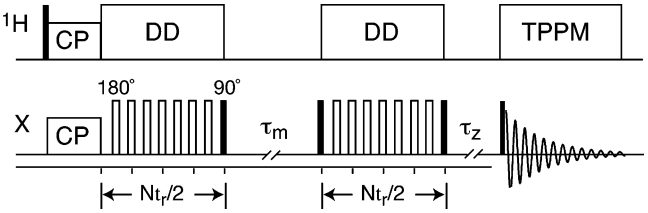

Figure 1. CODEX pulse sequence. Filled and open rectangles indicate 90° and 180° pulses, respectively. CP, cross polarization; DD, dipolar decoupling; TPPM, two-pulse phase modulation.[46]

NY). Typical radio frequency (rf) field strengths were 50 kHz for ^{19}F and ^{13}C and 60−70 kHz for ^{1}H. Recycle delays ranged from 1.5 to 3 s. Cross-polarization (CP) contact times were 300 μs for ^{19}F and 500 μs for ^{13}C experiments. ^{13}C and ^{19}F chemical shifts were referenced to the α-glycine ^{13}C′ signal at 176.49 ppm on the TMS scale and the Teflon ^{19}F signal at −122 ppm, respectively.

The pulse sequence for the ^{19}F and ^{13}C CODEX experiments is shown in Figure 1.[14] Two rotor-synchronized π-pulse trains recouple the CSA interaction under MAS. During the mixing time (τ_m), spin diffusion changes the chemical shift frequency and prevents complete refocusing of the stimulated echo. To correct for spin−lattice relaxation (T_1) effects during τ_m, a *z*-filter (τ_z) is added after the second π-pulse train. Two experiments, an exchange experiment (S) with the desired τ_m and a short τ_z (10 μs), and a reference experiment (S_0) with interchanged τ_m and τ_z, were conducted. The normalized intensity, S/S_0, was measured as a function of the mixing time until it reached a plateau. Error bars were propagated from the signal-to-noise ratios of the S_0 and S spectra.

Simulation of CODEX Curves. The τ_m-dependent CODEX curves were calculated in MATLAB using eqs 2−7 (below). *n*-dimensional rate matrices were constructed for oligomers of size *n*, where the rate constants are calculated according to eq 2. The mixing-time-dependent magnetization (t) was calculated using eq 7. For model compounds with known internuclear distances and dipolar couplings, best-fit simulation of the experimental exchange curve yields the overlap integral, $F(0)$. The best fit was obtained by minimizing the root-mean-square-deviation (RMSD) between the calculated intensity I_{sim} and the experimental intensity I_{exp} with respect to $F(0)$:

$$\mathrm{RMSD} = \sqrt{\sum_{i=1}^{N}(I_{\mathrm{sim},i} - I_{\mathrm{exp},i})^2/N} \qquad (1)$$

where N is the number of the data points in the exchange curve. The $F(0)$ values were incremented in 5 μs steps for ^{13}C CODEX and 1 μs steps for ^{19}F CODEX.

Structure Visualization and Modeling. The crystal structures of model compounds were obtained from the Cambridge Structure Databank and visualized in the software Mercury. The crystal structures of L-leucine and 5-^{19}F-L-tryptophan were directly measured by X-ray crystallography and confirmed to be consistent with the literature. The M2TMP structure was visualized and modeled in Insight II (Accelrys, San Diego, CA). The NMR-derived tetramer model (PDB accession code 1NYJ)[23] was used as a starting structure, with Ala30 replaced by Phe. To find tilt-angle-dependent interhelical F−F distances, we separately changed the tilt angle of each helix in the tetramer while fixing the position of Gly34, the middle of the helix. To define the new tilt angle, we first rotated the entire helical bundle together so that the helix to be modified was parallel to the screen. This helix was then rotated around the *z*-axis by either 38° or −38° so that it became vertical. The 38° angle is the ^{15}N NMR measured tilt angle of the M2 monomer. The vertical helix was then rotated by the desired new angle around the *z*-axis. This process was repeated for all the helices in the bundle. The rotation angle of the helices and the interhelical Gly34−Gly34 distances were unchanged in this procedure. The interhelical F−F distances at (4-^{19}F)Phe30 were then measured as a function of the tilt angle.

An alternative set of M2TMP structural models (courtesy of DeGrado, Howard, and co-workers) based on Cys scanning data[21] and EPR constraints[25] was also examined to obtain the interhelical F−F distances. The set of models contains helix tilt angles from 10° to 35° and was used without modification except for the A30F replacement.

3. Analysis of CODEX Curves by ^{1}H-Driven Spin Diffusion

In this section we describe the ^{1}H-driven spin diffusion theory used to fit the CODEX curve to determine distances. Since all samples used in our experiments are singly labeled with either ^{13}C′ or ^{19}F, magnetization exchange occurs between spins with identical isotropic chemical shifts but different shielding tensor orientations. Magnetization exchange among *n* such chemically equivalent but magnetically inequivalent sites reduces the intensity of the CSA echo to an equilibrium value of $1/n$.[15]

During the mixing time of a ^{1}H-driven spin diffusion experiment, polarization transfer between spins X_i and X_j occurs due to X_i-X_j dipolar coupling and is facilitated by the coupling of X to the abundant protons. The rate constant k_{ij} for this process under MAS rates slower than the ^{1}H−X dipolar coupling may be approximated by an equation derived for the static case:[26,27]

$$k_{ij} = 0.5\pi\omega_{ij}^{\ 2}F_{ij}(0) \qquad (2)$$

where ω_{ij} is the homonuclear dipolar coupling,

$$\omega_{ij} = \frac{\mu_0}{4\pi}\gamma^2\hbar\frac{1}{r_{ij}^{\ 3}}\frac{(1 - 3\cos^2\theta_{ij})}{2} \qquad (3)$$

which depends on the internuclear distance r_{ij} and the angle θ_{ij} between the internuclear vector and the external magnetic field. $F_{ij}(0)$ is the overlap integral describing the probability that single-quantum transitions occur at the same frequency for spins i and j:

$$F_{ij}(0) = \int_{-\infty}^{+\infty} f_i(\omega - \omega_i)\, f_j(\omega - \omega_j)\, \mathrm{d}\omega \qquad (4)$$

where $f_i(\omega - \omega_i)$ is the normalized single-quantum line shape of spin i in the absence of proton decoupling and ω_i is the center of the line shape. The overlap integral is related to the normalized zero-quantum line shape at zero frequency.[26]

For spin diffusion among *n* X spins, the time-evolution of the *n*-dimensional vector of the *z* magnetization, $\vec{M}(t)$, is given by

$$\frac{\mathrm{d}\vec{M}(t)}{\mathrm{d}t} = -\hat{\mathbf{K}}\vec{M}(t) \qquad (5)$$

where $\hat{\mathbf{K}}$ is the *n*-dimensional exchange matrix containing the rate constants k_{ij}. T_1 relaxation is not included in eq 5 since it is removed in the CODEX experiment by normalization of the exchange intensity S with the reference intensity S_0. Detailed balance of equilibrium magnetization requires that the sum of each column of the $\hat{\mathbf{K}}$ matrix be zero and that the rate constants satisfy $k_{ij} = k_{ji}$ for equal populations of equilibrium magnetiza-

(25) Duong-Ly, K. C.; Nanda, V.; DeGrado, W. F.; Howard, K. P. *Protein Sci.* **2005**, *14*, 856−861.
(26) Meier, B. H. *Adv. Magn. Opt. Reson.* **1994**, *18*, 1−115.
(27) Vanderhart, D. L. *J. Magn. Reson.* **1987**, *72*, 13−47.

tion.[28] Thus, for example, the exchange matrix of a four-spin system ABCD is

$$\hat{\mathbf{K}} = \begin{pmatrix} k_{AB}+k_{AC}+k_{AD} & -k_{BA} & -k_{CA} & -k_{DA} \\ -k_{AB} & k_{BA}+k_{BC}+k_{BD} & -k_{CB} & -k_{DB} \\ -k_{AC} & -k_{BC} & k_{CA}+k_{CB}+k_{CD} & -k_{DC} \\ -k_{AD} & -k_{BD} & -k_{CD} & k_{DA}+k_{DB}+k_{DC} \end{pmatrix} \quad (6)$$

The rate matrix approach includes not only direct but also relayed magnetization transfer effects. For example, the magnetization transfer from spin A to spin C is mediated not only by the matrix element $-k_{AC}$, which reflects the direct transfer, but also by $-k_{AB}$ and $-k_{BC}$, which reflect the relayed transfer pathway A → B → C.

The formal solution to eq 5 for a given initial magnetization distribution M(0) is

$$\vec{M}(t) = e^{-\hat{\mathbf{K}}t}\,\vec{M}(0) \quad (7)$$

The exponential operator can be treated by diagonalization of the $\hat{\mathbf{K}}$ matrix or calculated directly in a matrix-based software such as MATLAB. Expressed in terms of the diagonalized exchange matrix $\hat{\mathbf{D}}$,

$$\vec{M}(0) = \hat{R}\, e^{-\hat{\mathbf{D}}t}\, \hat{\mathbf{R}}^{-1}\, \vec{M}(0) \quad (8)$$

where $\hat{\mathbf{R}}$ is the eigenvector matrix of $\hat{\mathbf{K}}$. For an *n*-dimensional exchange matrix with zero-sum columns, it can be shown that one eigenvalue is always zero with the associated eigenvector this of $(1/\sqrt{n},1/\sqrt{n},...1/\sqrt{n})$, while all other eigenvalues of $\hat{\mathbf{K}}$ are positive. As a result, at large mixing times, $\vec{M}(0)$ approaches $(1/n,1/n,...1/n)$, corresponding to complete equilibration of the initial magnetization.

The distance-dependent dipolar coupling in eq 3 contains an angular term, $(1 - 3\cos^2\theta_{ij})$, that depends on the powder angles of individual molecules in the magnetic field. To simplify the analysis, the square of this term, which is relevant in the rate constant expression of eq 2, can be replaced by its powder-averaged value of 0.8.[27] For the singly labeled systems studied here, the overlap integral $F_{ij}(0)$ is approximated as the same for all spin pairs (*ij*), since the factors that influence the overlap integral — isotropic chemical shifts, chemical shift principal values, X−^{1}H dipolar couplings, and ^{1}H−^{1}H dipolar couplings[27] — are identical for all spins.

For the 100% ^{13}C- or ^{19}F-labeled crystalline small-molecule compounds, the dipolar coupling between magnetically inequivalent sites cannot be treated as due to isolated spin pairs, since multiple spins are present in the crystal lattice within dipolar-detectable distances.[29] We account for the multi-spin effect by replacing the ω_{ij}^2 term in eq 2 with its second moment $\sum_{m,n}\omega_{i_m,j_n}^2$. The dipolar couplings between all the *i* and *j* sites in $m \times n$ unit cells are summed until the coupling converges. For the small-molecule model compounds examined here, the second moment typically converges within a distance of ∼15 Å (involving about 20−90 unit cells) and exceeds the nearest-neighbor coupling by a factor of 2−43. The exact ratio of $\sum_{m,n}\omega_{i_m,j_n}^2/\omega_{ij}^2$ depends on the nearest neighbor distance, r_{ij}^{nn}: the longer the r_{ij}^{nn}, generally the more significant the second moment correction. For 4-^{19}F-2′-nitroacetanilide, which has a long r_{ij}^{nn} of 11.5 Å, the second moment exceeds the nearest neighbor ω_{ij}^2 by a factor of 43, making the effective coupling equivalent to an r_{ij}^{nn} of 6 Å rather than 11.5 Å. It should be noted that, since the labeling level is 100% for all the compounds, the dipolar second moment is the same for all labeled sites. This is a much simpler situation than spin diffusion in partially labeled or unlabeled samples, where the statistical nature of the nearest-neighbor distance creates a distribution of dipolar couplings and exchange rates.[29] For membrane peptides, long-range dipolar couplings between different aggregates are made negligible by lipid dilution. Thus, no second moment consideration is necessary, simplifying the extraction of the distances within an aggregate.

(28) Bain, A. D. *Prog. Nucl. Magn. Reson. Spectrosc.* **2003**, *43*, 63−103.

4. Results and Discussion

^{13}C′ CODEX of Model Compounds. We first analyze the ^{13}C′ CODEX spin diffusion data of ^{13}C′-labeled amino acids: α-Gly, γ-Gly, L-Leu, and L-Phe. These amino acids have two, three, or four magnetically inequivalent molecules in the respective unit cells, and thus should give equilibrium S/S_0 values of 0.50, 0.33, and 0.25. Figure 2a shows the τ_m-dependent S/S_0 values of α-Gly (Figure 2a) at 5 kHz MAS, reproduced from an earlier study.[13] A single-exponential decay with a time constant of 265 ms and an equilibrium value of 0.49 were found. α-Gly crystallizes in space group $P2_1/n$ and has four molecules in the unit cell divided into two pairs that are related by inversion symmetry.[30,31] The nearest-neighbor C′−C′ distance between the two inequivalent molecules is 4.22 Å. With a dipolar second moment that converges at a distance of 15 Å, the best fit yields an $F(0)$ value of 50 μs (Figure 2b,c).

γ-Gly crystallizes in the hexagonal space group $P3_2$ with three magnetically inequivalent molecules in the unit cell. The two nearest-neighbor C′−C′ distances are 4.17 Å.[32] The γ-Gly CODEX intensities (Figure 3a) exhibit a single-exponential decay with a time constant of 121 ms and the expected equilibrium value of 0.32. Using a dipolar second moment that converges within a distance of 15 Å,[32] the best-fit spin diffusion curve yields an $F(0)$ value of 120 μs (Figure 3b,c).

L-Leu and L-Phe both contain four orientationally unique molecules in the unit cell. L-Leu crystallizes in space group $P2_1$,[33,34] while L-Phe crystallizes in space group $P2_12_12_1$.[35] Leu has nearest-neighbor C′−C′ distances of 3.84, 5.59, and 6.01 Å, while Phe has much longer nearest-neighbor distances of 5.12, 11.0, and 14.0 Å. Consequently, the CODEX curves of the two compounds exhibit quite different decay rates. Leu gives rise to a biexponential decay with time constants of 23 ms and 415 ms (Figure 4a), while Phe has slower decays with time constants of 347 ms and 3.0 s (Table 1). The best-fit CODEX curve of Leu yields an $F(0)$ value of 50 μs (Figure 4b,c), while that of Phe gives an $F(0)$ value of 120 μs. The best-fit curve for Phe (not shown) does not fully capture the biexponential nature of the decay, which we attribute to the imperfection of the current theory for spin networks involving very different dipolar couplings or distances.

(29) Olender, Z.; Reichert, D.; Muller, A.; Zimmermann, H.; Poupko, R.; Luz, Z. *J. Magn. Reson. A* **1996**, *120*, 31−45.
(30) Jonsson, P.-G.; Kvick, A. *Acta Crystallogr.* **1972**, *B28*, 1827−1833.
(31) Marsh, R. E. *Acta Crystallogr.* **1958**, *11*, 654−663.
(32) Iitaka, Y. *Acta Crystallogr.* **1961**, *14*, 1−10.
(33) Gorbitz, C. H.; Dalhus, B. *Acta Crystallogr.* **1996**, *C52*, 1754−1756.
(34) Harding, M. M.; Howieson, R. M. *Acta Crystallogr.* **1976**, *B32*, 633−634.
(35) Al-karahouli, A. R.; Koetzle, T. F. *Acta Crystallogr.* **1975**, *B31*, 2461−2465.

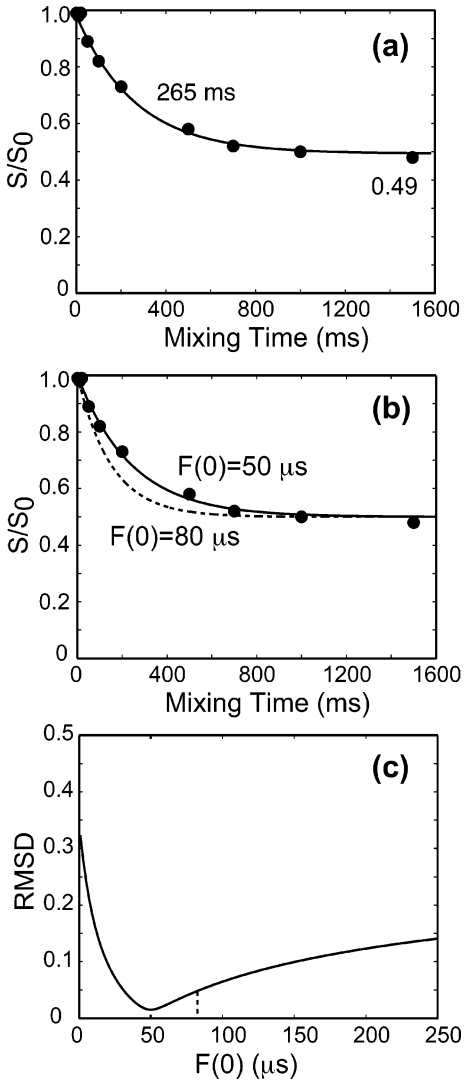

Figure 2. ^{13}C CODEX of ^{13}C′-α-Gly. (a) Experiment data (circles) are best fit to a single-exponential decay with a time constant of 265 ms. (b) Experimental data superimposed with the calculated magnetization exchange curves using the best-fit $F(0)$ of 50 μs (solid line) and the consensus $F(0)$ value of 80 μs (dashed line). (c) RMSD between the simulations and the experiment as a function of $F(0)$. Vertical dashed line indicates the RMSD for the consensus $F(0)$ value of 80 μs.

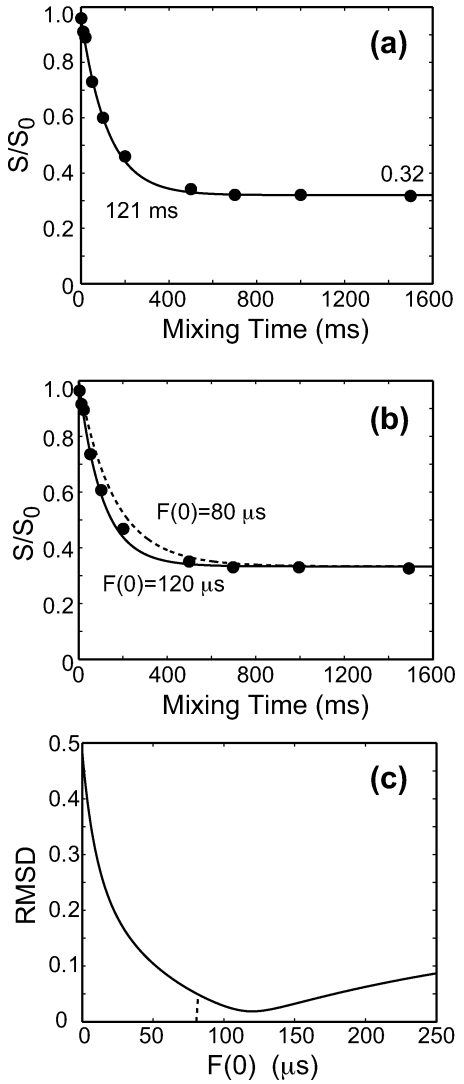

Figure 3. ^{13}C CODEX of ^{13}C′-γ-Gly. (a) The experimental data (circles) are best fit to a single-exponential decay with a time constant of 121 ms. (b) Experimental data superimposed with the calculated magnetization exchange curves using the best-fit $F(0)$ of 120 μs (solid line) and the consensus $F(0)$ of 80 μs (dashed line). (c) RMSD between the simulations and the experiment as a function of $F(0)$. Vertical dashed line indicates the RMSD for the consensus $F(0)$ value of 80 μs, which is close to that of the best-fit $F(0)$.

Table 1 summarizes the equilibrium values $(S/S_0)_{eq}$, exchange time constants τ_{SD}, and best-fit $F(0)$ values for the four ^{13}C′-labeled amino acids at 5 kHz MAS. The overlap integrals fall within a factor of 2.5. Since the spin-diffusion rate constant depends on $1/r^6$ but only linearly on $F(0)$ (eqs 2 and 3), the choice of an average $F(0)$ value of 80 μs introduces only a small distance uncertainty of less than 8%. The calculated ^{13}C′ CODEX curves for the various amino acids using this consensus $F(0)$ value are shown as dashed lines in Figures 2−4, panel b. In general, they fit the experimental data well and give low RMSD values close to the best-fit results.

The consensus ^{13}C′ $F(0)$ value of 80 μs is in approximate agreement with that obtained by Suter and Ernst on doubly carboxylic ^{13}C-labeled single-crystal malonic acid.[36] By direct measurement of the static ^{1}H-coupled zero-quantum spectra, the authors obtained zero-quantum T_2 relaxation times, T_2^{ZQ}, of 137 and 78.3 μs for two crystal orientations. Since $F(0) = T_2^{ZQ}/\pi$,[26] these correspond to overlap integrals of 44 and 25 μs, which are within a factor of 3 of our consensus $F(0)$ value.

The efficiency of ^{1}H-driven spin diffusion depends on the spinning speed: faster MAS attenuates spin diffusion and thus should give longer time constants and smaller $F(0)$ values. We investigated the effect of the spinning speed (ν_r) on $F(0)$ by measuring the ^{13}C′ CODEX curves at 2.5 and 10 kHz MAS. Figure 5 shows the CODEX curves at the three spinning speeds. Using overlap integral values scaled by $5000/\nu_r$ from the $F(0)$ value at 5 kHz MAS, we calculated the exchange curves for the two additional spinning speeds and found that they agree with the experimental data well (Figure 5). More exactly, the best-fit $F(0)$ values at the three MAS rates follow a $(1/\nu_r)^\beta$ dependence, where β varies between 0.5 and 0.9. This ν_r dependence is qualitatively consistent with the previously observed inverse ν_r dependence of the spin diffusion rate.[37]

(36) Suter, D.; Ernst, R. R. *Phys. Rev. B* **1985**, *32*, 5608−5627.

(37) Reichert, D.; Bonagamba, T. J.; Schmidt-Rohr, K. *J. Magn. Reson.* **2001**, *151*, 129−135.

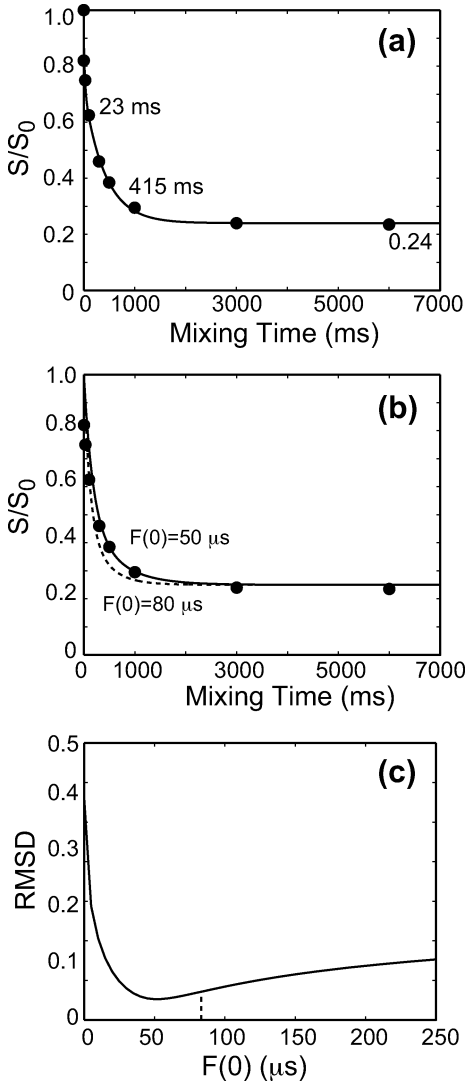

Figure 4. ^{13}C CODEX of ^{13}C′-Leu. (a) The experimental data (circles) are best fit to a biexponential decay with time constants of 23 and 415 ms. (b) Experimental data superimposed with the calculated magnetization exchange curves using the best-fit $F(0)$ of 50 μs (solid line) and the consensus $F(0)$ value of 80 μs (dashed line). (c) RMSD between the simulations and the experiment as a function of $F(0)$.

Table 1. Experimental Decay Constants and Best-Fit $F(0)$ Values of ^{13}C′ CODEX Data for Different Samples at Various Spinning Speeds

		2.5 kHz		5 kHz		10 kHz	
compd	$(S/S_0)_{eq}$[a]	τ_{SD} (ms)	$F(0)$ (μs)	τ_{SD} (ms)	$F(0)$ (μs)	τ_{SD} (ms)	$F(0)$ (μs)
α-Gly	0.47	139	90	265	50	477	35
γ-Gly	0.32	74	180	121	120	186	85
Leu	0.24	206[b]	70	261[b]	50	523[b]	35
Phe	0.28	na	na	347, 3000	120	na	na

[a] Equilibrium S/S_0 values were averaged from measurements at various spinning speeds. [b] These τ_{SD} values were obtained from stretched exponential fits to reflect the average decay constants.

^{19}F CODEX of Model Compounds. Compared to ^{13}C CODEX, ^{1}H-driven ^{19}F spin diffusion has two advantages: a longer distance reach due to the larger gyromagnetic ratio of ^{19}F, and higher angular sensitivity due to the larger ^{19}F CSA. We use two fluorinated compounds, 5-^{19}F-Trp and 4′-^{19}F-2′-nitroacetanilide, to measure the overlap integral of ^{19}F CODEX at 8 kHz MAS. Figure 6a−c shows the Trp data: an equilibrium

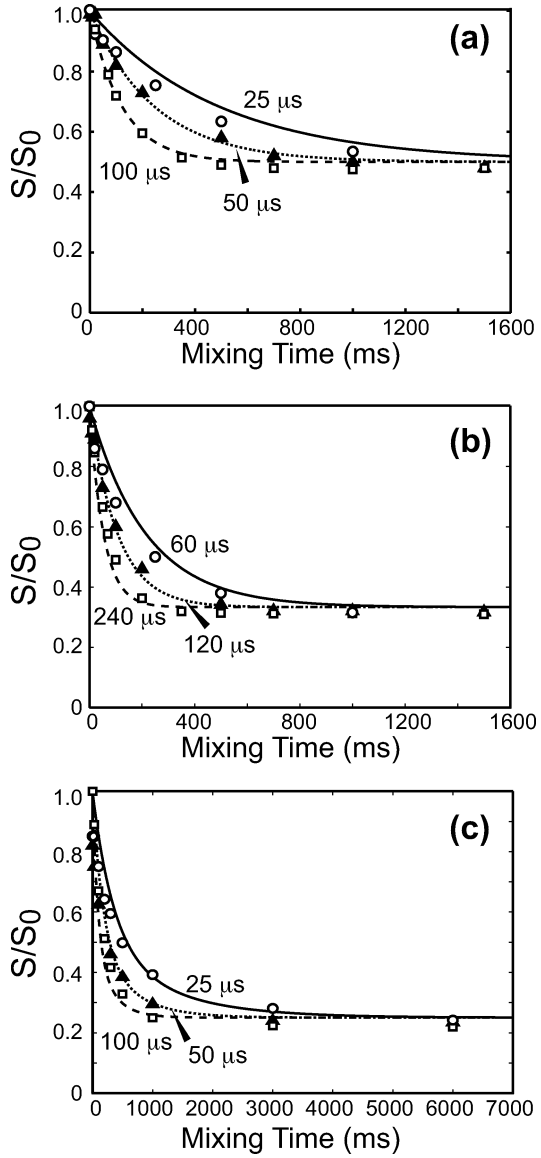

Figure 5. ^{13}C′ CODEX of (a) α-Gly, (b) γ-Gly, and (c) L-Leu at MAS rates of 10 (circles, solid line), 5 (triangles, dotted line), and 2.5 kHz (squares, dashed line). The best-fit $F(0)$ for the 5 kHz data of each sample is scaled by $5000/\nu_r$ to fit the data at the other two spinning speeds.

value of 0.50 and a τ_{SD} of 5.3 ms were found, consistent with the $P2_1$ space group of Trp (with two molecules in the unit cell).[38] The nearest-neighbor ^{19}F−^{19}F distance is 4.62 Å, giving a large dipolar coupling of 1.1 kHz, which explains the short time constant observed. The best fit is obtained with $F(0) = 28$ μs (Figure 6b,c), which is significantly smaller than the ^{13}C′ $F(0)$ values. This is reasonable since the instantaneous ^{19}F chemical shift overlap is smaller than the ^{13}C′ chemical shift overlap due to the larger ^{19}F CSA: the anisotropy parameter (δ) of 5-^{19}F-Trp is 48 ppm, or 18 kHz, which is almost twice that of the carbonyl carbons. For 4′-^{19}F-2′-nitroacetanilide,[39] the observed spin diffusion decay constant is 52 ms, or 10 times that of Trp. This is qualitatively consistent with the longer nearest-neighbor intermolecular F−F distance of 11.5 Å. Despite the large structural difference with Trp, the best-fit $F(0)$ value,

(38) Takigawa, T.; Ashida, T.; Sasada, Y.; Kakudo, M. *Bull. Chem. Soc. Jpn.* **1966**, *39*, 2369−2378.
(39) Qi, J.-Y.; Zhou, Z.-Y.; Liu, D.-S.; Chan, A. S. C. *Acta Crystallogr.* **2001**, *E57*, o675−o676.

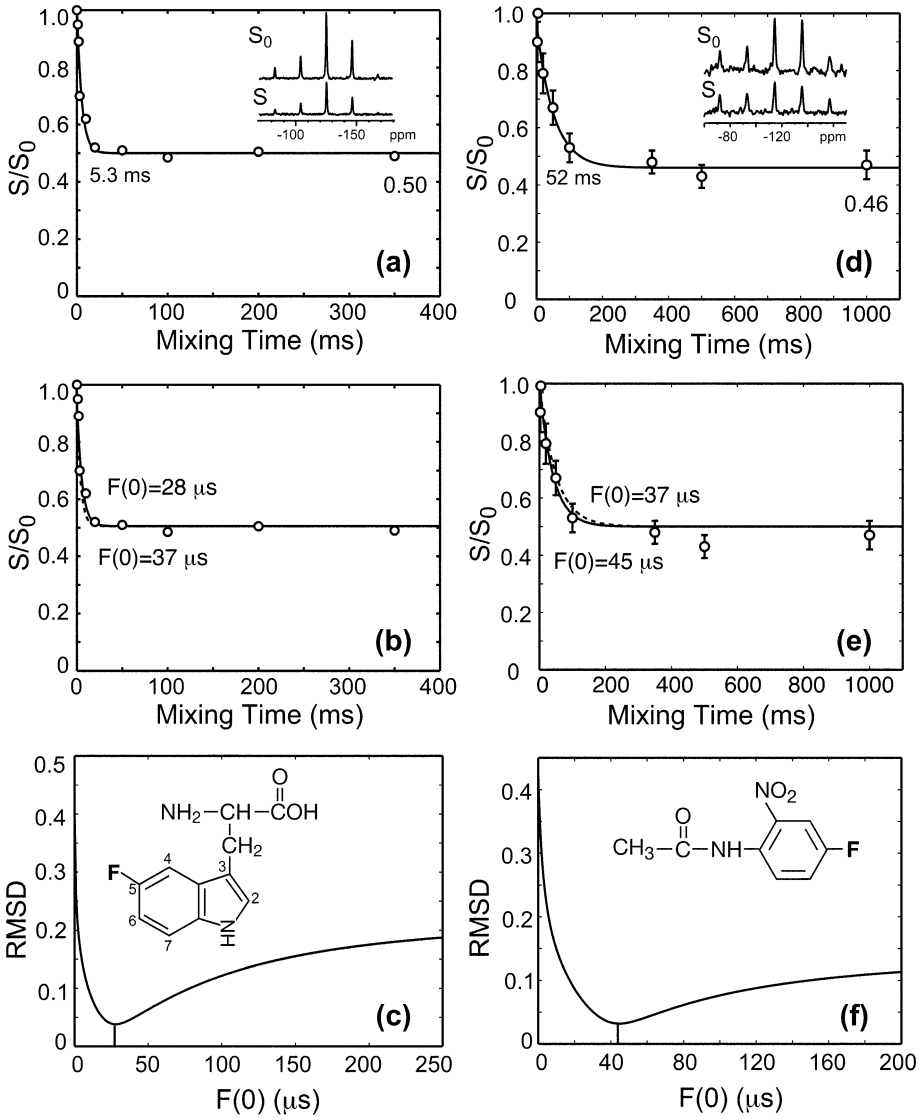

Figure 6. ^{19}F CODEX of 5-^{19}F-Trp (a−c) and 4′-^{19}F-2′-nitroacetanilide (d−f), whose chemical structures are shown in panels c and f. (a) The Trp data (circles) exhibit a single-exponential decay with a time constant of 5.3 ms and an equilibrium value of 0.50. (b) Calculated magnetization exchange curves using the best-fit $F(0)$ value of 28 μs (solid line) and the average $F(0)$ value of 37 μs (dashed line); both values agree with the experimental data well. (c) Trp RMSD between the simulation and the experiment as a function of $F(0)$. (d) ^{19}F CODEX data of 4′-^{19}F-2′-nitroacetanilide (circles), with a decay constant of 52 ms and an equilibrium value of 0.46. (e) The best-fit curve corresponds to an $F(0)$ of 45 μs (solid line), while the average $F(0)$ value of 37 μs (dashed line) still agrees with the data well. (f) RMSD as a function of $F(0)$ for 4′-^{19}F-2′-nitroacetanilide.

45 μs, is remarkably close to that of 5-^{19}F Trp. This confirms the existence of consensus $F(0)$ values under similar experimental conditions and validates our empirical approach of extracting the $F(0)$ value. We took the average $F(0)$ of 37 μs as the consensus value for ^{19}F CODEX at 8 kHz MAS. Simulations using this consensus value agree well with the experimental data of both compounds (Figure 6b,e).

^{19}F CODEX of M2TMP in Lipid Bilayers. With the $F(0)$ value known for ^{19}F CODEX at 8 kHz MAS, we can now determine F−F distances in structurally unknown systems such as M2TMP. Since the rate constant k_{ij} is proportional to $1/r^6$ but linear with $F(0)$ (eq 2), small variations in the $F(0)$ value do not affect the distance appreciably. In addition, for peptides diluted in lipid bilayers at molar concentrations of a few percent, the inter-oligomeric distances are several times longer than the intra-oligomeric distances, making the inter-oligomeric dipolar couplings more than 2 orders of magnitude smaller than the intra-oligomeric couplings. Thus, the second moment treatment for the single-component solids is unnecessary for two-component peptide−lipid mixtures, simplifying the analysis.

The ^{19}F CODEX experiments on M2TMP were carried out at 240 K, 56 K below the DMPC phase transition temperature (296 K) to eliminate slow peptide motion. Our previous experiments showed that, at this reduced temperature, slow motion is frozen, leaving dipolar spin diffusion as the only mechanism of exchange.[13] A CSA recoupling time, $N\tau_r$, of 0.25 ms was used, giving a $2\pi\delta N\tau_r$ of 13π (δ = 69 ppm). This is sufficiently large to detect orientational differences as small as $\sim 7°$.[40] Figure 7a shows the CODEX curve of M2TMP and a representative pair of spectra. Uncertainties in the S/S_0 values were propagated from the spectral signal-to-noise ratios and are small because of the high sensitivity of the spectra (Figure 7a inset). The S/S_0 value of the longest mixing time is 0.27, consistent with a tetrameric bundle. To fit the data, we first used a constrained biexponential function with a fixed equilib-

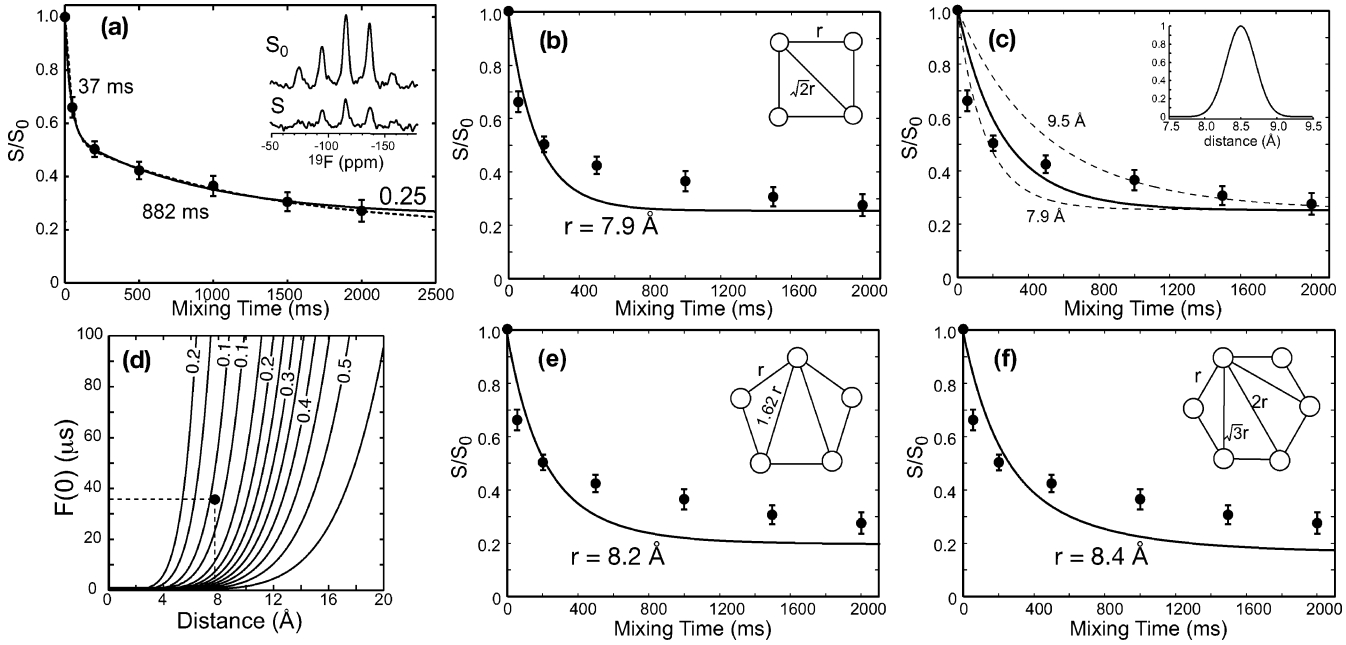

Figure 7. (a) ^{19}F CODEX data (circles) of M2TMP in DMPC bilayers at 240 K and 8 kHz MAS. The S_0 and S spectra for a mixing time of 1.0 s are shown. A biexponential fit with a fixed equilibrium value of 0.25 (solid line) shows excellent agreement with the data, with $R^2 = 0.9990$. Free fitting (dashed line) yields comparable decay constants and an equilibrium value of 0.20 ± 0.05 ($R^2 = 0.9995$). (b) Best-fit exchange curve using $F(0) = 37$ μs gives a nearest-neighbor F−F distance of 7.9 Å for a symmetric tetramer model, which is shown in the inset. (c) A Gaussian distance distribution centered at 8.5 Å (inset) for the same tetramer model gives a more balanced fit (solid line) to both the short and long time points. (d) RMSD between simulated and experimental CODEX curves as a function of distance r and $F(0)$. Contour levels vary from 0.10 to 0.55 in increments of 0.05. The minimum RMSD for $F(0) = 37$ μs is obtained at $r = 7.9$ Å (circle). (e) Best-fit CODEX exchange curve using a symmetric pentamer model deviates from the experimental equilibrium S/S_0 value. (f) Best-fit CODEX exchange curve using a symmetric hexamer model also deviates from the measured equilibrium S/S_0 value.

rium value of 0.25. The best-fit curve, $S/S_0 = 0.25 + 0.44\ e^{-t/37} + 0.31\ e^{-t/882}$ (solid line), shows excellent agreement with the experimental data ($R^2 = 0.999$), indicating that M2TMP forms tetrameric bundles in lipid bilayers, similar to when it binds to detergent micelles.[19,20]

Previous ^{15}N 2D dipolar-shift correlation spectra indicate that the M2TMP helical bundle is highly symmetric in lipid bilayers, since each ^{15}N label gives rise to a single ^{15}N peak.[22] This symmetry dictates that the four ^{19}F spins of Phe30 are located at the corners of a square, whose side r is the nearest-neighbor interhelical F−F distance between adjacent helices (Figure 7b inset). Using this symmetric tetramer model and the consensus $F(0)$ value of 37 μs, we simulated the experimental CODEX curve and found the best-fit at a F−F distance of 7.9 Å (Figure 7b). Figure 7d shows the 2D RMSD contour plot between the simulations and the experiment as a function of $F(0)$ and r. The contour lines are nearly parallel to the $F(0)$ axis, confirming that the fitting is much more sensitive to the distance r than to $F(0)$. The distance uncertainty, allowing for a conservative estimate of an $F(0)$ uncertainty of a factor of 2 on each side of the consensus value (i.e. 18−75 μs), amounts to only 0.8 Å.

The best-fit spin diffusion curve with $r = 7.9$ Å falls below the experimental intensities at 500 ms and 1 s (Figure 7b). This discrepancy reflects the biexponential nature of the experimental curve. Experiments at a lower temperature of 227 K gave the same S/S_0 values at short time points, thus verifying that no residual slow motion is present at 240 K to cause the fast initial decay. One possible reason for the biexponentiality of the curve is structural heterogeneity of the M2 helical bundle. Figure 7c shows that the calculated CODEX curve for 9.5 Å (upper dashed line) reproduces the long-time exchange intensities and is the upper bound that is still consistent with the experimental data. Thus, a conservative estimate of the interhelical F−F distance at A30F is 7.9−9.5 Å. Alternatively, simulation using a Gaussian distance distribution centered at 8.5 Å also gives a more balanced agreement with both the short and long time points of the experimental data (solid line, Figure 7c). Although a double Gaussian distribution centered at two different distances can better capture the biexponentiality of the curve, there is no good physical justification for a bimodal distance distribution, and the ^{19}F spectral line shape does not give any indication of two distinct conformations of the peptide. Another possible reason for the imperfection of the fit is the phenomenological nature of the ^{1}H-driven spin diffusion theory used to simulate the MAS data.

While the constrained biexponential fit of Figure 7a agrees with the data well, free fitting, on the other hand, gave an equilibrium value of 0.20 ± 0.05 (dashed line, Figure 7a). This implies that pentamers, with an expected equilibrium value of 0.20, and even hexamers, with an equilibrium value of 0.16, cannot be completely ruled out on the basis of the equilibrium S/S_0 value. Fortunately, the ambiguity can be resolved by calculating the CODEX curves for a symmetric pentamer (Figure 7e) and a symmetric hexamer (Figure 7f). We find that even the best-fit exchange curve in each model (obtained by varying r) deviates substantially from the experimental data at long times: the calculated equilibrium intensities fall below the measured values by more than the experimental uncertainty. Thus, a combination of the equilibrium value and the exchange time course is important for determining the oligomeric size of large aggregates, whose $1/n$ values become more difficult to distinguish from $1/(n+1)$ or $1/(n-1)$ as n increases.

(40) deAzevedo, E. R.; Bonagamba, T. J.; Hu, W.; Schmidt-Rohr, K. *J. Chem. Phys.* **2000**, *112*, 8988−9001.

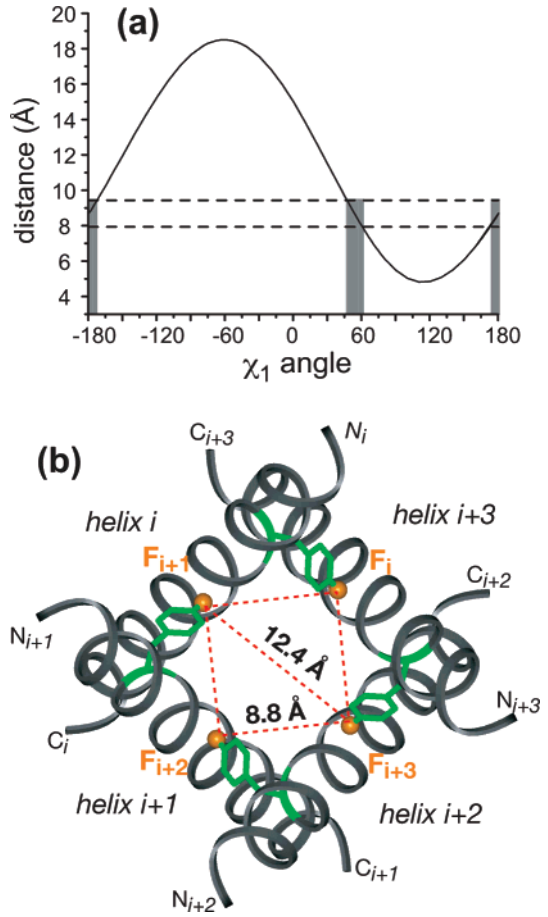

Figure 8. (a) $^{19}F-^{19}F$ distance between (4-^{19}F)Phe30 of adjacent helices as a function of Phe χ_1 angle in the NMR-derived model of M2TMP tetramer (PDB code 1NYJ). A distance of 7.9−9.5 Å is satisfied near χ_1 angles of +60° and +180°. However, the $\chi_1 = +60°$ rotamer causes severe steric conflicts between the side chain and the backbone and is thus ruled out. (b) Top view of the NMR-based M2TMP tetramer model with a nearest-neighbor $^{19}F-^{19}F$ distance of 8.8 Å at Phe30 between adjacent helices. The Phe ring of helix $i+1$ protrudes from its backbone and lies close to the neighboring helix i.

What is the structural implication of the interhelical Phe30−Phe30 distance of 7.9−9.5 Å? The intermolecular distance depends on a number of factors: the channel diameter, the helix orientation, and the Phe χ_1 torsion angle. We first assess the effect of the χ_1 angle on the distance. In the NMR-derived tetramer model (PDB accession code 1NYJ), the measured F−F distance can only be satisfied for $\chi_1 = +60°$ and 180° (Figure 8a). However, out of the three Phe χ_1 rotamers, $\chi_1 = +60°$ is energetically forbidden in α-helices due to steric conflicts between the aromatic ring and the backbone.[41,42] Thus, only the $\chi_1 = 180°$ rotamer agrees with the data. This is also the most favorable rotamer for Phe in α-helices.[41,42] With $\chi_1 = 180°$, the F−F distance between adjacent helices in the NMR-derived tetramer model is 8.8 Å, which agrees with the ^{19}F CODEX result within experimental uncertainty. Figure 8b shows a cross section of this tetramer model with the F−F distances highlighted. The Phe30 ring of helix $i+1$ protrudes from its backbone in a roughly perpendicular direction and lies close to the neighboring helix i (without causing steric conflicts). The distance between the opposing helices is 12.4 Å, which gives a measure of the diameter of the channel at this residue.

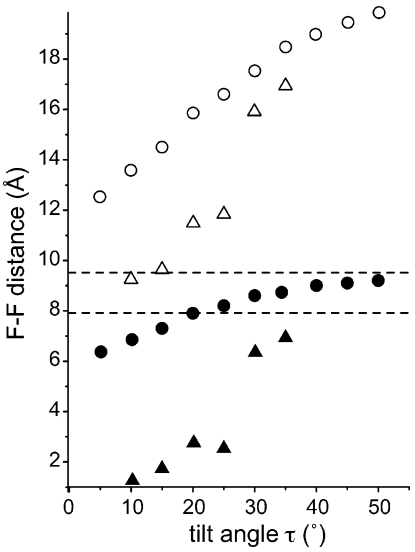

Figure 9. Phe30 $^{19}F-^{19}F$ distances between adjacent helices in the M2TMP tetramer as a function of the helix tilt angle for two different structural models: circles, ^{15}N NMR derived model; triangles, functional model based on Cys mutagenesis and EPR data. The $\chi_1 = 180°$ and $\chi_1 = -60°$ rotamers are shown as filled and open symbols, respectively. The F−F distance range determined from this study is delimited by the dashed lines.

With the Phe χ_1 conformation known, the measured F−F distance provides a valuable constraint to the orientation of the helices and the diameter of the helical bundle. We first examine the tilt angle dependence. Starting from the original NMR-derived tetramer model reported by Cross and co-workers,[22,23] which has a helix tilt angle of 38°, we varied the tilt angle while holding the channel diameter and the helix rotation angle constant. The rotation angle around the helix axis defines which residues face the channel interior versus the lipids. This information is well known qualitatively from functional studies of the M2 protein[21] and quantitatively from 2D ^{15}N NMR spectra of oriented membranes.[22] The interhelical Phe30 F−F distances are plotted in Figure 9 for the NMR model (filled circles). It can be seen that tilt angles less than 20° give distances outside the measured range of 7.9−9.5 Å and thus can be ruled out.

An alternative M2TMP tetramer model (designated as the functional model below) was proposed by DeGrado and co-workers on the basis of Cys scanning data.[21] The transmembrane segment of the intact protein was successively mutated to Cys, and the effects of the mutation on the reversal potential, ion currents, and amantadine resistance of the channel were measured. Fourier analysis of the data showed a periodicity that is consistent with a tetrameric helical bundle. This functional model was further refined by a recent EPR study of M2TMP in phosphatidylcholine membranes of different thicknesses.[25] By observing the dipolar line broadening of the spin label at the N-terminus of the helix, the authors found qualitative evidence that the distance between the N-termini of the helices decreases with increasing membrane thickness, suggesting that the M2TMP helices become less tilted in thicker membranes. Figure 9 plots the F−F distances for the different tilt angles of this functional model (triangles). The distance increases with increasing tilt angles as expected. At a small tilt angle such as 15°, a distance of 1.7 Å is found for $\chi_1 = 180°$ (filled triangles), which is clearly unphysical. At this helix tilt, a χ_1 angle of −60°

(41) Lovell, S. C.; Word, J. M.; Richardson, J. S.; Richardson, D. C. *Proteins: Struct., Funct., Genet.* **2000**, *40*, 389−408.
(42) Janin, J.; Wodak, S. *J. Mol. Biol.* **1978**, *125*, 375−386.

gives a F−F distance of 10 Å, which is more reasonable but still inconsistent with the ^{19}F CODEX result. Thus, small tilt angles can also be ruled out in this functional model. At the largest tilt angle of 35°, the trans rotamer gives a F−F distance of 7.0 Å, which still falls short of the measured value by ∼1.0 Å. While larger tilt angles would better agree with the experimental data, they would create unfavorable hydrophobic mismatch between the peptide and the lipid bilayer. An examination of the backbone structure of this functional model indicates that the channel diameter, as defined by the backbone−backbone distances, is comparable to or even slightly larger than the channel diameter in the NMR-derived structural model. Thus, the channel diameter does not explain the short Phe30 F−F distance in the functional model. However, the rotation angle around the helical axis is slightly different between the NMR model and this functional model. This small difference causes the Phe side chain in the functional model to extend more into the center of the channel and is sufficient to give rise to the 1.8 Å shorter distance compared to the NMR model (8.8 Å) at a helix tilt of ∼35°.

Clearly, to uniquely determine both the interhelical separation and the peptide orientation, one needs to measure multiple interhelical distances at multiple residues. The Phe30 F−F distance measurement shown here is only the first demonstration of the rich information content of such long-range intermolecular distance restraints. By determining distances in the 10 Å range, this anisotropic magnetization exchange technique complements other NMR distance methods such as rotational resonance that have been used to determine peptide interfacial structure.[43] The present ^{1}H-driven ^{19}F spin diffusion experiment can also be compared with a ^{19}F radio-frequency-driven recoupling (RFDR) experiment, which yielded F−F distances of 5−12 Å on model compounds with an accuracy of 1−2 Å.[44] However, the RFDR experiment does not allow spin counting and measures distances between chemically distinct fluorinated groups, and thus it is less applicable to amino acids. Distance extraction from RFDR exchange curves also requires an adjustable simulation parameter, the zero-quantum relaxation time, T_2^{ZQ}, which is analogous to the spectral overlap function considered here.[26]

Compared to other spectroscopic probes such as EPR and fluorescence resonance energy transfer, the current ^{19}F CODEX NMR method has the advantages that the label is relatively nonperturbing to the protein and does not introduce extra degrees of freedom to the distances of interest. Therefore, it promises to be a new and general probe for the oligomeric structure of membrane proteins.

5. Conclusion

We have shown that ^{1}H-driven spin diffusion between spins with identical isotropic shifts but different anisotropic shifts, CODEX, not only allows spin counting but also provides long-range distance constraints in oligomeric membrane peptides. Using a rate matrix analysis, in which the spin diffusion rate constant is proportional to the overlap integral and the square of the dipolar coupling, we determined consensus overlap integral values from the CODEX curves of structurally known model compounds. For ^{13}C′-labeled amino acids at 5 kHz MAS, a consensus $F(0)$ value of 80 μs was found. For aromatic ^{19}F-labeled compounds at 8 kHz MAS, a consensus $F(0)$ value of 37 μs was obtained. Using ^{19}F CODEX, we proved for the first time that the M2 transmembrane peptide of influenza A virus forms tetramers in lipid bilayers. Moreover, the nearest-neighbor interhelical F−F distance between Phe30 residues is 7.9−9.5 Å. This supports the M2TMP tetramer model obtained from NMR orientational constraints and indicates that the helix tilt angle must be greater than 20° in DMPC bilayers. In addition, the experimental F−F distance points out a subtle difference in the helix rotation angle between the functional model and the NMR-based model of M2TMP. This difference propagates to a detectably shorter side-chain F−F distance predicted by the functional model than the experimental result. Thus, the long-range CODEX intermolecular distances are useful for refining the high-resolution oligomeric structure of membrane peptides.

The CODEX technique and analysis can be applied to both membrane-bound proteins and protein aggregates outside the membrane[45] to determine oligomeric numbers and intermolecular distances in the 10 Å range. These intermolecular distances complement local structural parameters such as torsion angles and intramolecular distances in elucidating the full three-dimensional structure of complex biological assemblies.

Acknowledgment. This work is supported by a NSF CAREER grant to M.H. The authors thank Rajeswari Mani for various help in sample preparation and NMR experiments, and Prof. W. DeGrado and Prof. K. Howard for generously sharing the coordinates of their M2 structure models.

JA0603406

(43) Smith, S. O.; Song, D.; Shekar, S.; Groesbeek, M.; Ziliox, M.; Aimoto, S. *Biochemistry* **2001**, *40*, 6553−6558.
(44) Gilchrist Jr, M. L.; Monde, K.; Tomita, Y.; Iwashita, T.; Nakanishi, K.; McDermott, A. E. *J. Magn. Reson.* **2001**, *152*, 1−6.
(45) Antzutkin, O. N.; Balbach, J. J.; Leapman, R. D.; Rizzo, N. W.; Reed, J.; Tycko, R. *Proc. Natl. Acad. Sci. U.S.A.* **2000**, *97*, 13045−13050.
(46) Bennett, A. E.; Rienstra, C. M.; Auger, M.; Lakshmi, K. V.; Griffin, R. G. *J. Chem. Phys.* **1995**, *103*, 6951−6958.